

# RSC Advances



This is an *Accepted Manuscript*, which has been through the Royal Society of Chemistry peer review process and has been accepted for publication.

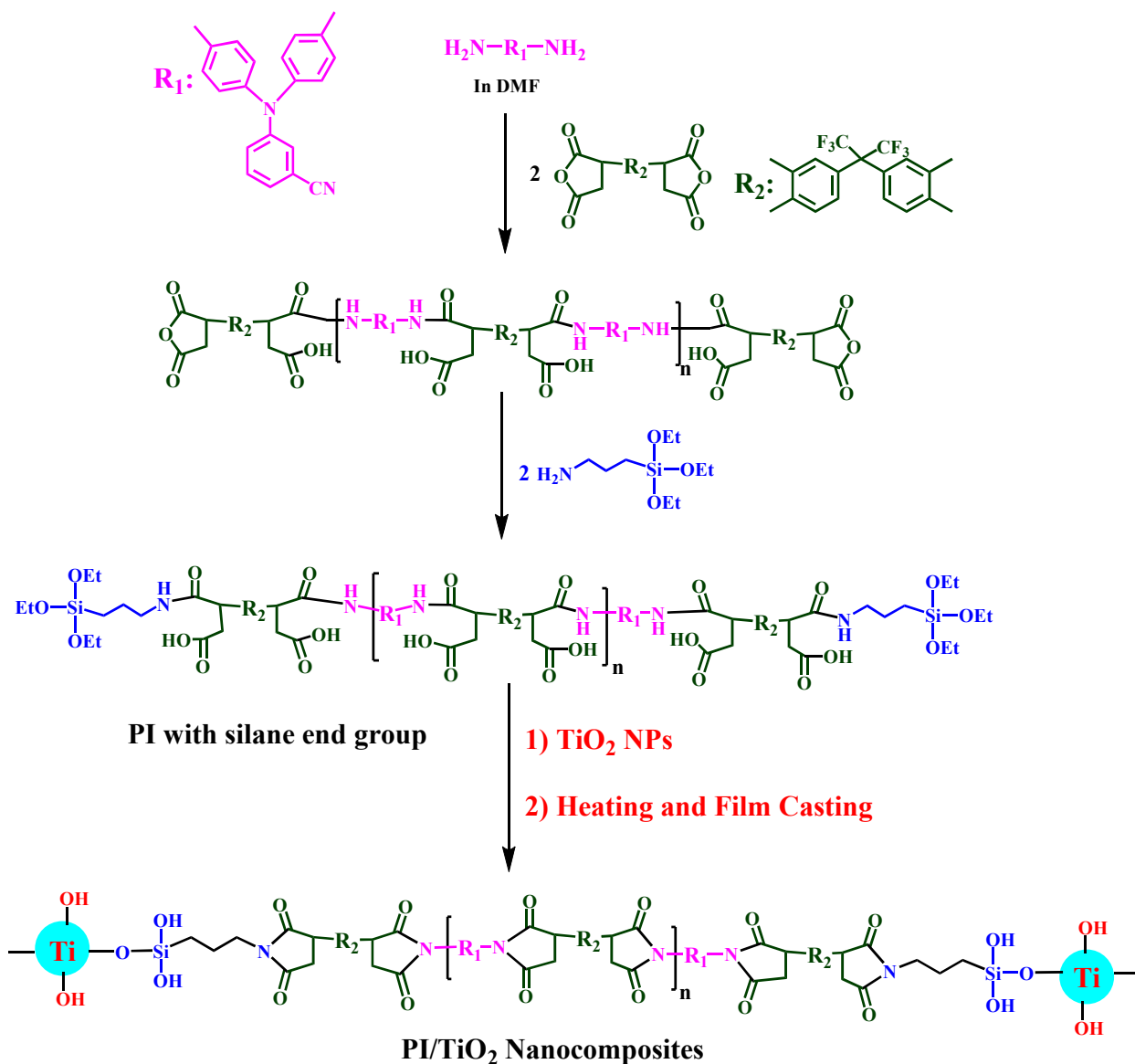
*Accepted Manuscripts* are published online shortly after acceptance, before technical editing, formatting and proof reading. Using this free service, authors can make their results available to the community, in citable form, before we publish the edited article. This *Accepted Manuscript* will be replaced by the edited, formatted and paginated article as soon as this is available.

You can find more information about *Accepted Manuscripts* in the [Information for Authors](#).

Please note that technical editing may introduce minor changes to the text and/or graphics, which may alter content. The journal's standard [Terms & Conditions](#) and the [Ethical guidelines](#) still apply. In no event shall the Royal Society of Chemistry be held responsible for any errors or omissions in this *Accepted Manuscript* or any consequences arising from the use of any information it contains.

## Graphical Abstract

Thermal, mechanical and optical transport properties of nanocomposite materials based on triethoxysilane-terminated polyimide and TiO<sub>2</sub> nanoparticles



Novel polyimide/TiO<sub>2</sub> nanocomposites with good mechanical, optical and thermal properties were prepared by the incorporation of TiO<sub>2</sub> nanoparticles into silane terminated polyimide.



# Thermal, mechanical and optical transport properties of nanocomposite materials based on triethoxysilane-terminated polyimide and TiO<sub>2</sub> nanoparticles

Mohammad Dinari <sup>\*</sup>, Parvin Asadi

*Department of Chemistry, Isfahan University of Technology, Isfahan 84156-83111, Iran*

## Abstract

---

\* - Corresponding author. Tel.: +98 3133913270; fax: +98 3133912351.

E-mail address: [dinari@cc.iut.ac.ir](mailto:dinari@cc.iut.ac.ir); [mdinary@gmail.com](mailto:mdinary@gmail.com)

In the preparation of polymer based nanocomposites (NCs), compatibility between organic phase and inorganic nanoparticles as filler can be improved by a variety of methods, such as functionalizing polymer chains at their ends, adding a coupling agent to bond polymer chains and inorganic network and etc. in this study, several novel polyimide/titanium dioxide nanocomposites (PI/TiO<sub>2</sub> NCs) were prepared by the incorporation of TiO<sub>2</sub> nanoparticles into silane terminated PI. To this point, firstly, 3-(bis(4-aminophenyl)amino)benzotrile as a diamine monomer was synthesized and then it was reacted with an excess amount of 4,4'-(hexafluoroisopropylidene) diphthalic anhydride. The triethoxysilane terminal groups were introduced by reacting the anhydride end-groups of the polymer with (3-aminopropyl)-triethoxysilane. Different hybrid materials based on the silane-terminated PI with inorganic TiO<sub>2</sub> network were successfully fabricated by thermal imidization. The resulting materials were characterized by different techniques. According to the transmission electron microscopy images, the TiO<sub>2</sub> nanoparticles were well dispersed into the PI matrix with particle size around 20-40 nm. The resulting composite's mechanical, optical and thermal properties are effectively enhanced by the incorporation of 8wt.% TiO<sub>2</sub> nanoparticles. According to the thermogravimetric analysis curves, the T<sub>5%</sub> of the NC was increased with the TiO<sub>2</sub> loading and approximately 63 °C improvements in T<sub>5%</sub> is found. The tensile strength of the hybrid films is significantly increased compared with the pure PI.

*Keywords:* Benzotrile linkages; Silane terminated polyimide; TiO<sub>2</sub> nanoparticles; Tensile strength; Optical properties

## 1. Introduction

Polymeric materials have many applications in multiple industries but improvements in processability, durability and performance are required for their use in aerospace power and propulsion components.<sup>1-5</sup> Forming hybrid polymer composites with small amount of inorganic nanoparticles (NPs) is a promising approach to obtain balanced properties by exploiting the advantages of both organic polymer and inorganic NPs and the properties of the resulting nanocomposites (NCs) can dramatically improved.<sup>6-8</sup> In recent years, the synthesis of polymer NCs as new materials has attracted a considerable attention since they possess novel optical, electronic, gas barrier, mechanical, and magnetic properties.<sup>9-11</sup> Inorganic NPs exhibit excellent thermal stability and high modulus. A diversity of crystalline materials, i.e., three dimensional nano metal oxides, two-dimensional layered silicates, and one-dimensional carbon nanotubes, have been used for reinforcement of the polymer matrixes.<sup>12,13</sup> In addition to nanoclay and carbon nanotubes, oxide NPs are emerging fillers for many applications. Titanium dioxide (TiO<sub>2</sub>) are one of the most used inorganic NPs owing to its low cost, biocompatibility, low toxicity, UV shielding effect and photocatalytic properties.<sup>14</sup> This NP offer favorable mechanical strength, thermal stability, and high surface area and as a result, it has been extensively studied in many polymeric materials.<sup>15-21</sup>

Aromatic polyimides (PIs) are a well-known class of high performance polymers that combine high thermal stability with chemical resistance, displaying excellent electrical and mechanical properties. Due to these characteristics, PIs have found extensive applications as fibers, films, coatings, photoresists, and composites.<sup>22-24</sup> However, the synthesis and processing of these polymers are difficult because of their limited solubility and infusibility.<sup>25</sup> To overcome these drawbacks, considerable efforts have been made to improve the processability of such polymers, while maintaining their remarkable properties.<sup>26</sup> The most common strategy consists

in the incorporation of flexible alkyl side chains, non-coplanar biphenylene moieties and bulky lateral substituent on the rigid polymer backbones.<sup>27-30</sup> Among these, the introduction of bulky pendant units is a simple and convenient way to enhance the solubility and to incorporate new chemical functionalities.<sup>30</sup> In order to induce certain features to the final PIs, while maintaining their intrinsic characteristics such as outstanding thermal stability and mechanical strength one way is designing new diamine or dianhydride monomers with novel molecular structures. According to the previous study by introducing of functional nitrile groups in the PI backbone, the thermooxidative resistance and the dielectric constant relative to the polymers may be increased in comparison to those macromolecular without this substituent on to the chain.<sup>31,32</sup> Also, the nitrile substituent may increase other physical properties of high performance materials, since it was shown that some amorphous polymers containing strong dipoles displayed piezoelectric response.<sup>31-33</sup>

In the preparation of PI NCs, compatibility between organic polymer and inorganic NPs can be enhanced by a variety of methods, such as functionalizing polymer chains at their ends, selecting appropriate groups of polymers within the repeat units, adding a coupling agent to bond PI chains and inorganic network.<sup>34-37</sup> However, it is still a challenge to homogeneously disperse inorganic phase in polymer matrices in a highly efficient and controllable way. In continues to these researches, herein, we wish to report the preparation of new PI/TiO<sub>2</sub> NCs using 3-aminopropyl triethoxysilane (APTEOS) functionalized PI. The Si-OEt end groups could condense with TiO<sub>2</sub> NPs and provide organic-inorganic hybrids. For this purpose, a diamine monomer containing *N*-benzoylnitrile side chain was designed and synthesized. A novel silane terminated-PI film and related PI/TiO<sub>2</sub> NCs were prepared via polycondensation reaction of the synthesized diamine and 4,4'-(hexafluoroisopropylidene) diphthalic anhydride (6FDA). The

resulting materials were characterized by different techniques and it is hoped that the benzonitrile-containing PI will have enhanced processability as well as thermal stability.

## 2. Experimental

### 2.1. Materials

All materials and solvents were purchased from Merck Chemical Co and Aldrich Chemical CO. 3-Aminobenzonitrile, 1-fluoro-4-nitrobenzene, 6FDA, APTEOS, palladium on activated carbon (10 wt%) and hydrazine hydrates were used as received. *N*-methyl-2-pyrrolidone (NMP), *N,N*-dimethylformamide (DMF) and *N,N'*-dimethylacetamide (DMAc) were dried over barium oxide, followed by fractional distillation. Nanosized TiO<sub>2</sub> powder was purchased from Nanosabz Co. (Tehran, Iran) with average particle sizes of 30-50 nm.

### 2.2. Synthesis of diamine monomer

Diamine 2 was synthesis according to our previous article.<sup>33</sup> In brief, at first, 3-(bis(4-nitrophenyl)amino)benzonitrile (1) was prepared by nucleophilic substitution reaction of 3-aminobenzonitrile with 1-fluoro-4-nitrobenzene in the present of cesium fluoride according to Scheme 1. This compound was purified by re-crystallization from acetic acid to dinitro intermediate 1 in 90% yield; mp: 218-220 °C. Than aromatic diamine 2 having a benzonitrile pendent group, 3-(bis(4-aminophenyl)amino)benzonitrile, was successfully synthesized by hydrazine Pd/C-catalytic reduction. The crude product was recrystallized from ethanol and dried in vacuum at 80 °C. The yield was 81%; mp 188-191 °C. The purity of monomer 2 was checked by thin layer chromatography, which showed one spot in an ethylacetate/cyclohexane mixture (50:50) with R<sub>f</sub>=0.42.

FTIR (KBr, cm<sup>-1</sup>) of diamine 2: 3448 (s), 3377 (s), 3113 (w), 3075 (w), 2225 (s), 1555 (m), 1535 (m) 1440 (w), 1323 (w), 1252 (w), 844 (m), 739 (w). <sup>1</sup>H-NMR (400 MHz, DMSO-*d*<sub>6</sub>,

ppm) of diamine 2: 4.49 (s, 4H, NH), 6.26-6.28 (d, 8H, Ar-H,  $J= 4.5$  Hz), 6.49 (s, 1H, Ar-H), 6.76-6.78 (d, 1H, Ar-H), 7.19-7.20 (d, 1H, Ar-H,  $J= 4$  Hz), 7.36-7.38 (dd, 1H, Ar-H,  $J= 4$  Hz).  $^{13}\text{C}$ -NMR (100 MHz, DMSO- $d_6$ ), of diamine 2,  $\delta$  (ppm): 108.22 (Ar), 112.31 (CN), 118.82 (Ar), 121.18 (Ar), 123.32 (Ar), 124.12 (Ar), 125.17 (Ar), 137.25 (Ar), 138.45 (Ar), 141.35 (Ar), 148.33 (Ar). Elemental analysis calculated for  $\text{C}_{19}\text{H}_{16}\text{N}_4$  ( $300.36\text{ g mol}^{-1}$ ): Calcd. (%) C, 75.98%; N, 18.65 %; H, 5.37 %. Found (%) C, 75.86%; N, 18.79%; H, 5.39 %.

### Scheme 1

#### 2.3. Preparation of polyamic acid (PAA) and pristine PI

3-(Bis(4-aminophenyl)amino)benzotrile (1.00 g, 3.32 mmol) as diamine monomer 2 was dissolved in NMP (20 wt%) and cooled with the ice water bath. After completely dissolved, 6FDA (1.47 g, 3.32 mmol) as the anhydride monomer 3 was added into the above solution under stirring with a mechanical stirrer, a condenser and a nitrogen inlet for 6 h at room temperature (R.T.) to obtain the polyamic acid (PAA) as shown in Scheme 2. The inherent viscosity of the PAA was 0.97 dL/g, as measured in DMAc at a concentration of 0.5 g/dL at 30 °C. The PAA was converted into PI by thermal imidization method. In the method, about 2.00 g of the PAA solution was spread into a Petri culture dish 7 cm in diameter and baked at 90 °C overnight (ca. 12 h) for the removal of the casting solvent. The semidried PAA film was further dried and converted into the PI by sequential heating at 150 °C for 30 min, at 200 °C for 30 min, and at 250 °C for 1 h. The inherent viscosity of the PI was 1.13 dL/g at a concentration of 0.5 g dL $^{-1}$ .

FT-IR (KBr,  $\text{cm}^{-1}$ ) of the PI: 3086 (aromatic C-H stretching), 2225 (stretching  $\text{C}\equiv\text{N}$ ), 1777 (asymmetric imide  $\text{C}=\text{O}$  stretching), 1722 (symmetric imide  $\text{C}=\text{O}$  stretching), 1625 (aromatic  $\text{C}=\text{C}$  stretching), 1236, 1126 (C-F stretching), and 821 (C-N bending).  $^1\text{H}$ -NMR (400 MHz, DMSO- $d_6$ , ppm) of the PI: 6.26-6.27 (d, 2H, Ar-H,  $J= 3.5$ ), 6.48-6.49 (s, 2H, Ar-H,  $J= 4.5$

Hz), 6.68-7.69 (d, 2H, Ar-H,  $J= 4.5$  Hz), 6.88 (s, 1H, Ar-H), 7.27-7.28 (d, 1H, Ar-H,  $J= 3.5$ ), 7.36-7.37 (d, 1H, Ar-H,  $J= 3.5$ ), 7.17-7.18 (d, 1H, Ar-H,  $J= 4.5$  Hz), 7.66-7.68 (d, 1H, Ar-H,  $J= 3.5$ ), 7.88-7.89 (d, 1H, Ar-H,  $J= 4.5$  Hz), 8.17-8.18 (d, 1H, Ar-H,  $J= 4.5$  Hz), 8.38-8.39 (d, 1H, Ar-H,  $J= 4.5$  Hz). Anal. Calcd. for  $C_{38}H_{18}F_6N_4 O_4$  (708.56 g/mol ): C, 64.42%; H, 2.56%; N, 7.91%; Found: C, 64.48%; H, 2.53%; N, 7.85%.

## Scheme 2

### 2.4. Preparation of the silane terminated-PI/TiO<sub>2</sub> NC films

In the preparation of PI based NCs, compatibility between organic PI and inorganic NPs can be enhanced by a variety of methods, such as functionalizing polymer chains at their ends, selecting appropriate groups of polymers within the repeat units, adding a coupling agent to bond PI chains and inorganic network. Silane-terminated PI/TiO<sub>2</sub> hybrid films were synthesized according to the synthesis pathway as shown in Scheme 3. In this way, 3-(bis(4-aminophenyl)amino)benzotrile (1.00 g, 3.32 mmol) was dissolved in NMP (20 wt%) and cooled with the ice water bath. After completely dissolved, 6FDA (2.94 g, 6.64 mmol) was added into the above solution under stirring for 6 h at room temperature to formed the PAA solution. In the next step APTEOS (0.74 g, 3.32 mmol) was slowly dropped into the mixture. The reaction was stirred at room temperature for 6 h to obtain the PAA with triethoxysilane-terminated groups as shown in Scheme 3. Then different amount of TiO<sub>2</sub> NPs (4, 8 and 12wt.%) were added to the PAA solution and thin films of PI with different percentages of TiO<sub>2</sub> NPs were fabricated by casting onto dust-free glass plates. Resulted thin films were annealed using an electric air-circulating oven at 60, 120, 170, 220, and 270°C for 1 h each and 300°C for 6 h and then were cooled and removed from glass surface using a sharp edge blade. The obtained films were around 30-40  $\mu\text{m}$  thick and were used for further characterization. The NCs are named as

PI/TiO<sub>2</sub> NC4%, PI/TiO<sub>2</sub> NC8% and PI/TiO<sub>2</sub> NC12%, where the percentage given in the genetic abbreviations is the weight percentage.

### Scheme 3

#### 2.5. Techniques

Fourier transform infrared (FT-IR) spectroscopic measurements were performed using a Magna-IR Nicolet 560 FTIR spectrophotometer by incorporating samples in KBr disks. The spectra were recorded in the range of 4000–400 cm<sup>-1</sup> at a resolution of 4 cm<sup>-1</sup>. Carbon, hydrogen and nitrogen content of the compounds were determined by pyrolysis method by Vario EL elemental analyzer. NMR spectra were recorded on a Bruker Avance DRX 400 and 100MHz, by using solutions in deuterated dimethylsulfoxide (DMSO-d<sub>6</sub>). Inherent viscosity ( $\eta_{inh}$ ) of the polymer in DMAc was measured at about 0.5 g/dL concentration with an Ubbelohde viscometer at 30±0.5 °C. The XRD patterns were collected by using a Philips Xpert MPD X-ray diffractometer. The diffractograms were measured for 2 $\theta$ , in the range of 10–80°, using a voltage of 40 kV and Cu K $\alpha$  incident beam ( $\lambda=1.51418$  Å). Thermal stability was measured with a TGA-2950 thermo gravimetric analyzer (TA instrument Co.) at a heating rate of 20 °C min<sup>-1</sup> from room temperature to 800 °C under a continuous flow of nitrogen. Tensile strength and elongation at break of thin PI membranes were measured with the help of UTM-INSTRON, PLUS, Model No. 8800. Test samples with dimension of 10×25 mm<sup>2</sup> and thickness in the range of 30–40µm were used for the measurement of tensile strength and percentage of elongation at break. Ultra violet spectra of the polymer films were recorded at room temperature using Detector SD–2000 (Ocean Optics Inc.) and source lamp DH–2000.

### 3. Results and discussion

#### 3.1. FT-IR and NMR study

FT-IR,  $^1\text{H-NMR}$  and  $^{13}\text{C-NMR}$  spectra of the dinitro 1 and diamine 2 were reported in our previous article.<sup>33</sup> In the FT-IR spectrum of the dinitro compound 1, the nitro group show two characteristic bands at around 1541 and 1338  $\text{cm}^{-1}$  for  $\text{NO}_2$  asymmetric and symmetric stretching, respectively. After reduction, the characteristic absorptions of the nitro group disappeared and the amino group showed the typical N-H stretching absorption pair in the region of 3448-3377  $\text{cm}^{-1}$ . The characteristic absorptions of the nitrile group were observed at 2225  $\text{cm}^{-1}$ . In  $^1\text{H-NMR}$  spectrum of the diamine compound 2, a peak at 4.50 ppm was assigned to the amine protons group and all aromatic protons appeared at 6.25-7.38 ppm.

Conversion of the PAA to the fully cyclized PI was proved by means of by FT-IR,  $^1\text{H-NMR}$  spectroscopy and elemental analysis techniques. The FT-IR spectra of the PAA and corresponding PI based on 6FDA are presented in Fig. 1. Neat PAA showed a broad absorption characteristic band of carboxylic O-H and amide N-H groups at about 2600-3700  $\text{cm}^{-1}$  and a narrow characteristic band at 1685  $\text{cm}^{-1}$  associated to C=O of amide linkages (Fig. 1a). In the spectra of PI, absorption bands of the imide groups appear at 1777 and 1722  $\text{cm}^{-1}$  for the symmetric and anti-symmetric stretching vibrations of the carbonyl groups. Other characteristic absorption bands of the imide were appeared at 1353 and 702  $\text{cm}^{-1}$  for the C-N stretching and C=O bending, respectively. Moreover, it is observed in Fig. 2c that the stretching vibration at about 1220~1100  $\text{cm}^{-1}$  and weak absorption band at 689  $\text{cm}^{-1}$  were assigned to the C-F group and  $\text{CF}_2$  groups, respectively.<sup>38</sup>

**Fig. 1**

Figs. 2 exhibits a  $^1\text{H-NMR}$  spectra of the PI based on 6FDA, in which all the peaks have been readily assigned to the hydrogen atoms of the repeating unit and no amide or acid protons at 10-12 ppm were appeared. This indicates that complete imidization was really achieved. The

assignments of each proton designated in the  $^1\text{H-NMR}$  spectrum are in complete agreement with the proposed polymer structures and PAA was converted into PI by chemical imidization. The sharp peaks at 4.50 ppm corresponding to the amine protons in  $^1\text{H-NMR}$  spectrum of diamine disappear completely here, and new peaks were appeared at 7.50-8.40 ppm correspond to the protons in the dianhydride units (Fig. 2).

**Fig. 2**

The structures of the PI and hybrid composites were characterized by FT-IR spectra. Fig. 3 shows the FT-IR spectra of the pure  $\text{TiO}_2$  NP, PI and NC materials with different amount of  $\text{TiO}_2$  NPs. Neat  $\text{TiO}_2$  show the characteristic peak of hydroxyl group at  $3423\text{ cm}^{-1}$  and the Ti-O-Ti bands are appeared in the range of  $450\text{-}650\text{ cm}^{-1}$  (Fig. 3a).<sup>18,19</sup> For the NCs containing triethoxysilane-terminated PI and inorganic  $\text{TiO}_2$  NPs, in addition to the PI peaks (Fig. 3d), the FT-IR spectra show new absorption bands at  $1020\text{-}1100\text{ cm}^{-1}$  for Si-O-Ti symmetric stretching vibrations and at  $890\text{ cm}^{-1}$  for Si-OH groups.<sup>19</sup> The bands at  $2880\text{-}2930\text{ cm}^{-1}$  can be ascribed to the C-H symmetrical and asymmetrical stretching absorptions of the  $\text{CH}_2$  group of the APTES, respectively. Also, the Ti-O-Si bands are appeared in the range of  $450\text{-}650\text{ cm}^{-1}$  in the FT-IR spectra of the NC films (Fig. 3b and 3c). This result verifies that inorganic  $\text{TiO}_2$  NPs were successfully formed in the hybrid PI composites by the thermal imidization techniques.

**Fig. 3**

### 3. 2. X-ray diffraction

Fig. 4 shows the XRD patterns of the pristine titania, PI matrix and NCs with different  $\text{TiO}_2$  percentage. For neat  $\text{TiO}_2$  (Fig. 4a), the peaks appeared at 101, 110, 004, 200, 105, 211, 204, 220, 301 were for the crystalline portion of this compound.<sup>28</sup> The XRD analysis for the pure PI film exhibits a typical amorphous structure, which is associated with the broad peak of  $2\theta$  at  $20^\circ$

in the range from  $15^{\circ}$  to  $25^{\circ}$  (Fig. 4b). The PI/TiO<sub>2</sub> films, on the other hand, show additional sharp diffraction peaks superimposed on top of the broad amorphous background. The XRD patterns of PI/TiO<sub>2</sub> NCs with 4, 8 and 12wt.% of TiO<sub>2</sub> NPs indicating that the morphology of TiO<sub>2</sub> NPs has not been disturbed during the process. The intensity of peaks corresponding to TiO<sub>2</sub> NPs increased with higher concentration of TiO<sub>2</sub> in the obtained NCs. All these data indicated that TiO<sub>2</sub> NPs were dispersed in the polymer matrix.

**Fig. 4**

### 3.3. Morphology of PI and NCs

The morphology of the silane terminated PI with 4, 8 and 12wt% of TiO<sub>2</sub> NPs was monitored with FE-SEM technique as shown in Fig. 5. The silica loading and reinforcement binding with PI matrix are confirmed by the morphology. From FE-SEM images, any aggregation or phase separation has not been observed. This shows the method for the preparation of silane terminated PI/TiO<sub>2</sub> NCs used in this study could make the inorganic part well dispersed into polymer matrix and gave uniform and homogeneous distribution of TiO<sub>2</sub> NPs in these NCs as compared with PI without end group silane coupling agent.<sup>38</sup> As discussed above, the triethoxysilane terminal groups of PI can inhibit strong phase separation tendency between organic PI and inorganic TiO<sub>2</sub> NPs. Even for the high TiO<sub>2</sub> concentration, PI/TiO<sub>2</sub> NC12% still can prevent the significant phase separation of titania and lead to a homogenous distribution of TiO<sub>2</sub> NPs (Fig. 5e and 5f).

**Fig. 5**

Fig. 6 shows the TEM micrographs of silane terminated PI NC with 4 and 12wt% of TiO<sub>2</sub> NPs. In these images, no aggregation is visible between the modified TiO<sub>2</sub> NPs and relatively satisfactory dispersion of NPs can be observed in comparison with PI without using silane coupling agent by in situ polymerization.<sup>39</sup> The above observation confirms that triethoxysilane

terminal groups introduced by the reaction with APTEOS are important to counter-balance the phase separation tendency when the TiO<sub>2</sub> content is too high. As shown in TEM images, it was estimated that the particle size of the TiO<sub>2</sub> NPs in the NC materials PIs are around 20-40 nm with spherical shapes.

### Fig. 6

#### 3.4. Mechanical properties of PI films

The effects of TiO<sub>2</sub> NPs loading on the tensile properties of silane terminated PI/TiO<sub>2</sub> NPs films were investigated and the results are presented in Fig. 7. Filler consisting entirely of TiO<sub>2</sub> generally increases the ultimate strength, but decreases the maximum extensibility. The mechanical properties of NCs largely depend on the external load transfer between the reinforcing nanofiller phase and the matrix.<sup>40-42</sup> According to the previous study,<sup>43</sup> the strength should be reduced if there are no bonding sites between the organic polymer phase and the inorganic TiO<sub>2</sub> phase due to the inert nature of the PIs and the weak interactions between these polymers and the TiO<sub>2</sub>. In this case, the TiO<sub>2</sub> acts as nonreactive and non-reinforcing filler. It is generally believed that external stress on a polymer composite is transferred from the continuous phase (polymer matrix) to the discontinuous phase (filler). Therefore, the ultimate properties of the NCs are dependent on the extent of bonding between the two phases, the surface area of the TiO<sub>2</sub>, and the arrangements between the TiO<sub>2</sub> particles. As can be seen in Fig. 7, the tensile strength of PI/TiO<sub>2</sub> NPs films is significantly increased compared with the pure PI. The maximum stress at break (ultimate strength) was found to increase initially with increase in TiO<sub>2</sub> content, and at 8 wt% TiO<sub>2</sub> showed a maximum value of 112.41 MPa (relative to the 96.23 MPa of the neat PI) representing considerable improvement in tensile strength. As the TiO<sub>2</sub> content increases (12 wt.%), the tensile strength of PI/TiO<sub>2</sub> films decreases, but still better than the pure

PI film because of increasing brittleness. According to the Fig. 7., ultimate strength and initial modulus were increased with TiO<sub>2</sub> contents, but ultimate elongation decreased with the increase of TiO<sub>2</sub> contents, especially at higher TiO<sub>2</sub> content. For elongation at break, the sample geometry (most importantly the film thickness) is an additional factor to consider and may be the determine factor why the 8% wt% TiO<sub>2</sub> sample shows the best result.<sup>44</sup> The above results showed that the interactions between the silane terminated PI and the TiO<sub>2</sub> are very important.

### Fig. 7

#### 3.5. Thermal properties

The thermal stability of silane terminated PI/TiO<sub>2</sub> NCs and pure PI as references was investigated at the heating rate of 20 °C min<sup>-1</sup> from 20 to 800 °C. Fig. 8 shows TGA curves for the four samples pure PI, PI/TiO<sub>2</sub> NC4%, PI/TiO<sub>2</sub> NC8% and PI/TiO<sub>2</sub> NC12%. The pure PI film, is quite stable up to 420 °C. The weight of the pure PI film remained around 98% under 450 °C, and then substantially decreased from 480 °C to 600 °C (Fig. 8). The PI/TiO<sub>2</sub> NC film showed a similar pattern of weight loss but at higher temperature (over 500 °C) than the pure PI films and the decomposition was completed at around 600 °C. The decomposition temperature at 5% (T<sub>5%</sub>) weight loss for these composites increases with the TiO<sub>2</sub> nanofillers loading. About 63 °C improvements in T<sub>5%</sub> is found in 10 wt% TiO<sub>2</sub> nanofillers loading. Excellent thermal stability should be attributed to the contribution of the existed covalent bonding interaction between silane terminated PI and TiO<sub>2</sub> nanofillers. The 10% weight loss temperatures (T<sub>10%</sub>) of the silane terminated PI is 513 °C and for NC materials with 4, 8 and 12wt% of TiO<sub>2</sub> nanofillers, it is 530, 564 and 576 °C, respectively (Table 1). The char yields at 800 °C of the NCs with different TiO<sub>2</sub> content are higher than that of pure PI which provided more evidence of completely organic-inorganic bonding.<sup>45</sup> The char yield of NCs was from 76 to 80% at 800 °C. By comparison of the

thermal properties of these hybrid materials with different NCs with similar structures,<sup>28,30</sup> the results show that these hybrids had higher thermal stability because of the good interaction between the silane terminated PI and TiO<sub>2</sub> NPs. Hence, incorporation of the PI with reactive terminal groups showed ability to prevent the phase separation of TiO<sub>2</sub> in PI matrices due to the strong covalent and partial hydrogen bonding networks formed during the process and the thermal properties was enhanced.

**Fig. 8**

**Table 1**

### *3.6. Optical properties of the PI and composites*

It is known that aromatic PI films, owing to their high glass-transition and decomposition temperature, low water absorption, good transmission and low optical loss, are excellent candidates for use as transparent flexible substrates in displays or other electronic applications.<sup>46</sup> Thin films of PI and NC with different TiO<sub>2</sub> NPs were used for optical transparency with UV-vis spectroscopy. Fig. 9 exhibits the UV-vis transmittance spectra of these hybrid films. UV-vis absorption spectra of PI/TiO<sub>2</sub> hybrid films showed a maximum absorption at 390 nm. Silane terminated PI shows the highest transmittance of 97% at 480 nm, and the film is entirely colorless. After incorporating TiO<sub>2</sub> NPs with weight percentage from 4% to 12% into silane terminated PI, the composite films kept transparent and uniform appearance, and their transmittance was only slightly decreased (Fig. 9). The light scattering and opacity caused by aggregated inorganic titania phases in the wavelength scale were effectively avoided for the films, which is attributed to the reaction between triethoxysilane terminal groups of polymer and TiO<sub>2</sub> NPs as compared with other PI/TiO<sub>2</sub> NC films.<sup>47</sup> The UV shielding ability relates with the scattering and/or absorbance of TiO<sub>2</sub> NPs. The scattering property plays a main role in shielding

of UV irradiation. Thus, these PI/TiO<sub>2</sub> hybrid films have potential to apply as coating to block the UV radiation, particularly between 370-400 nm. Most PI between the UV and visible area show strong absorption due to the highly conjugated aromatic structures and intermolecular charge-transfer complex formation of PI.<sup>48</sup> According to the Fig. 9, the percentage of transmittance at 500 nm for neat PI is 98% and for NC with different amount of TiO<sub>2</sub> NP, it is around 89-96%. All NCs showed highest optical transparency due to the presence of trifluoromethyl groups in anhydride part, because these groups are very much effective in decreasing charge transfer complex formation and improve the optical properties of the resulting hybrid materials.<sup>48-50</sup>

**Fig. 9**

#### **4. Conclusion**

In the preparation of polymer based NCs, compatibility between organic phase as a matrix and inorganic NPs as filler can be improved by a variety of methods, such as functionalizing polymer chains at their ends, adding a coupling agent to bond polymer chains and inorganic network and etc. In this study, first, new silane-terminated PI with benzonitrile pendant group was synthesized by the reacting of the anhydride end groups of the polymer with APTEOS. Then, a series of PI NC films based on the triethoxysilane-terminated PI and different amount of inorganic TiO<sub>2</sub> NPs (4, 8 and 12wt.%) was successfully fabricated by thermal imidization techniques. The formation of the resulting NCs was confirmed by the FT-IR and XRD techniques. According to the FE-SEM and TEM images, the TiO<sub>2</sub> NPs were well dispersed into the PI matrix and no aggregation was observed because the triethoxysilane terminal groups of PI can inhibit strong phase separation tendency between organic PI and inorganic TiO<sub>2</sub> NPs. The size of the TiO<sub>2</sub> NPs in the NC materials was around 20-40 nm with spherical shapes. The tensile strength of PI/TiO<sub>2</sub> NPs

films is significantly increased compared with the pure PI and the maximum stress at break was found to increase initially with increase in TiO<sub>2</sub> content, and at 8wt% TiO<sub>2</sub> showed a maximum value of 112.41 MPa relative to the 96.23 MPa of the neat PI. According to the TGA curves, the T<sub>5%</sub> of the NC was increased with the TiO<sub>2</sub> nanofillers loading and approximately 63 °C improvements in T<sub>5%</sub> is found in 8wt% TiO<sub>2</sub> nanofillers loading. Excellent thermal stability should be ascribed to the role of the existed covalent bonding interaction and or hydrogen bonding between silane terminated PI and TiO<sub>2</sub> nanofillers. Neat PI and related NC films show good optical transparency due to the presence -CF<sub>3</sub> groups in anhydride part. According to the obtained results, the resulting hybrid materials due to their good thermal, mechanical, optical and morphological properties, are amenable for use as high-performance materials and demonstrate a promising potential for future application.

### Notes

The authors declare no competing financial interest.

### Acknowledgements

We wish to express our gratitude to the Research Affairs Division Isfahan University of Technology (IUT), Isfahan, for partial financial support. Further financial support from National Elite Foundation (NEF), and Iran Nanotechnology Initiative Council (INIC) is gratefully acknowledged.

### References

- 1 W. E. Moerner, S. M. Silence, *Chem. Rev.*, 1994, **94**, 127-155.
- 2 Z. M. Dang, Y. Q. Lin, H. P. Xu, C. Y. Shi, S. T. Li, J. Bai, *Adv. Funct. Mater.*, 2008, **18**, 1509-1517.

- 3 N. Awang, A. F. Ismail, J. Jaafar, T. Matsuura, H. Junoh, M. H. D. Othman, M. A. Rahman, *React. Funct. Polym.*, 2015, **86**, 248-258.
- 4 C. Constantinescu, A. Rotaru, A. Nedelcea, M. Dinescu, *Mater. Sci. Semicon. Proc.*, 2015, **30**, 242-249.
- 5 M. Thelakkat, *Macromol. Materd. Eng.*, 2002, **287**, 442-461.
- 6 A. C. Balazs, T. Emrick, T. P. Russell, *Science*, 2006, **314**, 1107-1110.
- 7 S. Gong, Z. H. Zhu, S. A. Meguid, *Polymer*, 2015, **56**, 498-506.
- 8 R. Gines, R. Libanori, A. R. Studart, A. Bergamini, M. Motavalli, P. Ermanni, *Composites Part B.*, 2015, **72**, 80-86.
- 9 S. Thomas, G. Zaikov, V. Meera, *Recent advances in polymer nanocomposites: Synthesis and characterizations*, 2010 by CRC Press.
- 10 E. Ruiz-Hitzky, M. Darder, A. C. S. Alcântara, B. Wicklein, P. Aranda, *Adv. Polym. Sci.*, 2015, **267**, 39-86.
- 11 A. Kafy, K. K. Sadasivuni, H. C. Kim, A. Akther, J. Kim, *Phys. Chem. Chem. Phys.*, 2015, **17**, 5923-5931.
- 12 F. Wypych, K. G. Satyanarayana, *J. Colloid Interface Sci.*, 2005, **285**, 532-543.
- 13 S. Khaled, R. Sui, P. A. Charpentier, A. S. Rizkalla, *Langmuir*, 2007, **23**, 3988-3995.
- 14 R. J. Nussbaumer, W. R. Caseri, P. Smith, T. Tervoort, *Macromol. Mater. Eng.*, 2003, **288**, 44-49.
- 15 N. Nakayama, T. Hayashi, *J. Appl. Polym. Sci.*, 2007, **105**, 3662-3672.
- 16 P. C. Chiang, W.T. Whang, *Polymer*, 2015, **62**, 1-10.
- 17 H. Seyedjamali, A. Pirisedigh, *Colloid Polym. Sci.*, 2011, **289**, 15-20.
- 18 S. Mallakpour, M. Dinari, *Prog. Org. Coat.*, 2012, **75**, 373-378.

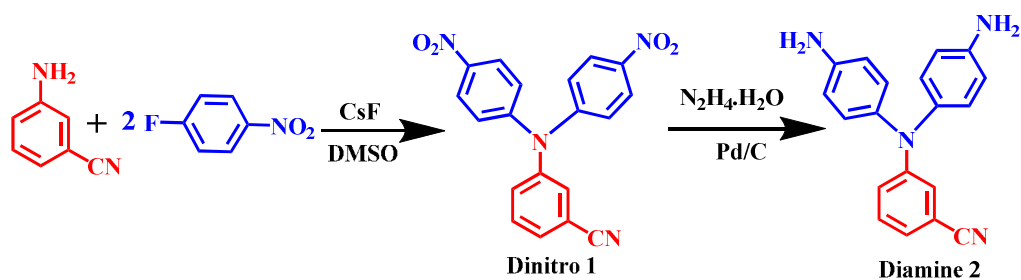
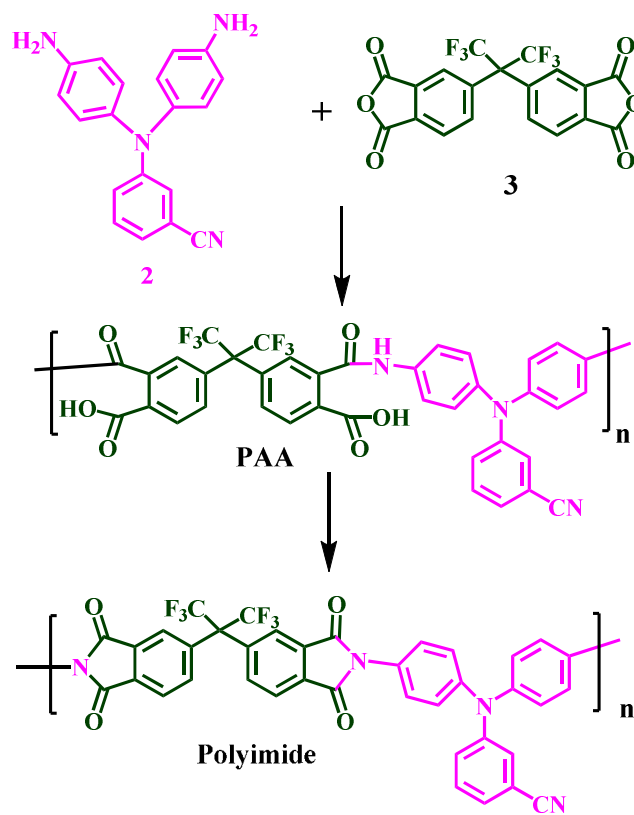
- 19 S. Mallakpour, P. Asadi, *Polym. Bull.*, 2012, **68**, 53-67.
- 20 Q. F. Xu, Y. Liu, F. J. Lin, B. Mondal A. M. Lyons, *ACS Appl. Mater. Interfaces*, 2013, **5**, 8915-8924.
- 21 H. Zhang, J. Huang, L. Yang, R. Chen, W. Zou, X. Lin, J. Qu, *RSC Adv.*, 2015, **5**, 4639-4647.
- 22 D. Yu, A. Gharavi, L. Yu, *J. Am. Chem. Soc.*, 1995, **117**, 11680-11686.
- 23 MK Ghosh, KL Mittal, *Polyimides: Fundamentals and Applications*, Marcel Dekker Inc., New York, USA 1996.
- 24 D. P. Erhard, F. Richter, C. B. A. Bartz, H. W. Schmidt, *Macromol. Rapid Commun.*, 2015, **36**, 520-527.
- 25 H. S. Hsiao, Y. T. Chou, *Polymer*, 2014, **55**, 2411-2421.
- 26 Y. T. Chern, J. Y. Tsai, *Macromolecules*, 2008, **41**, 9556-9564.
- 27 SH Hsiao, HM Wang, WJ Chen, TM Lee, C. M. Leu, *J. Polym. Sci. Part A: Polym. Chem.*, 2011, **49**, 3109-3120.
- 28 M. Dinari, H. Ahmadizadegan, *Polymer*, 2014, **55**, 6252-6260.
- 29 L. Yi, C. Li, W. Huang, D. Yan, *J. Polym. Res.*, 2014, **12**, 572-581.
- 30 M. Dinari, H. Ahmadizadegan, *RSC Adv.*, 2015, **5**, 8630-8639.
- 31 M. Bruma, F. Mercer, B. Schulz, R. Dietel, J. Fitch, P. Cassidy, *High Perform. Polym.*, 1994, **6**, 183-191.
- 32 B. Lin, X. Xu, *Polym. Bull.*, 2007, **59**, 243-250.
- 33 M. Dinari, H. Ahmadizadegan, *RSC Adv.*, 2015, **5**, 26040-26050.
- 34 C. F. Cheng, H. H. Cheng, P. W. Cheng, Y. J. Lee, *Macromolecules*, 2006, **39**, 7583-7590.
- 35 J. Liu, Y. Nakamura, T. Ogura, Y. Shibasaki, S. Ando, M. Ueda, *Chem. Mater.*, 2008, **20**, 273-281.

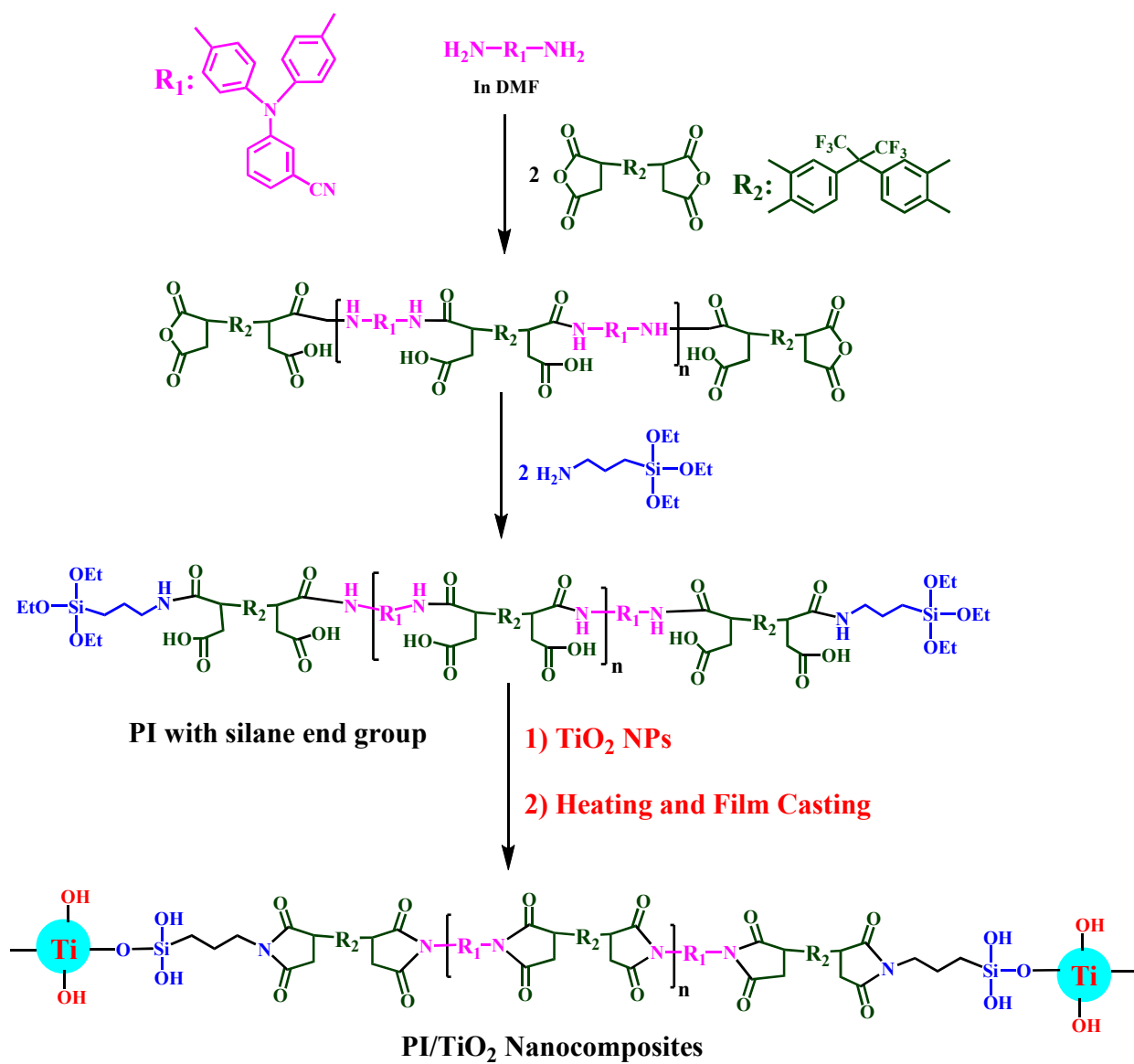
- 36 S. K. Kim, X. Wang, S. Ando, X. Wang, *Eur. Polym. J.*, 2015, **64**, 206-214.
- 37 Z. Xiao, P. Guo, C. Wang. *Colloid Polym. Sci.*, 2015, **293**, 307-312.
- 38 Y. Feng, J. Yin, M. Chen, M. Song, B. Su, Q. Lei, *Mater. Letters*, 2013, **96**, 113-116.
- 39 X. Liu, J. Yin, Y. Kong, M. Chen, Y. F, K. Yan, X. Li, B. Su, Q. Lei. *Thin Solid Films*, 2013, **544**, 352-356.
- 40 D. Qian, E. C. Dickey, R. Andrews, T. Rantell, *Appl. Phys. Lett.*, 2000, **76**, 2868-2870.
- 41 V. Antonucci, K. T. Hsiao, S. G. Advani, Review of polymer composites with carbon nanotubes. In; *Advanced Polymeric Materials Structure Property Relationships*; G. O. Shonaike, S. G. Advani, Eds.; CRC Press: Boca Raton, 2003.
- 42 S. M. Khaled, R. Sui, P. A. Charpentier, A. S. Rizkalla, *Langmuir*, 2007, **23**, 3988-3995.
- 43 S. Mallakpour, M. Dinari, *Polymer*, 2011, **52**, 2514-2523.
- 44 M. Chen, J. Yin, R. Jin, L. Yao, B. Sua, Q. Lei. *Thin Solid Films*, 2015, **584**, 233-237.
- 45 H. J. Yen, C. L. Tsai, P. H. Wang, J. J. Lin, G. S. Liou, *RSC Adv.*, 2013, **3**, 17048-17056.
- 46 M. D. Damaceanu, C. P. Constantin, A. Nicolescu, M. Bruma, N. Belomoina, R.S. Begunov. *Eur. Polym. J.*, 2014, **50**, 200-213.
- 47 J. Liu, Y. Nakamura, T. Ogura, Y. Shibasaki, S. Ando, M. Ueda, *Chem. Mater.* 2008, **20**, 273-281.
- 48 C. P. Yang, S. H. Hsiao, K. H. Chen, *Polymer*, 2002, **43**, 5095-5104.
- 49 W. Jang, D. Shin, S. Choi, S. Park, H. Han, *Polymer*, 2007, **48**, 2130-2143.
50. V. Kute and S. Banerjee, *J. Appl. Polym. Sci.*, 2007, **103**, 3025-3044.

### Caption for Schemes

**Scheme 1.** Synthesis of diamine with benzonitrile pendant group.

**Scheme 2.** Synthesis of PAA and PI.

**Scheme 3.** Synthesis of silane-terminated PI and PI/TiO<sub>2</sub> NC materials.**Scheme 1****Scheme 2**



Scheme 3

**Table 1**

Thermal properties of the pure PI and NC with different amount of TiO<sub>2</sub> NPs.

Samples	Decomposition temperature (°C)		Char yield (%) <sup>b</sup>
	T <sub>5</sub> <sup>a</sup>	T <sub>10</sub> <sup>a</sup>	
Pure PI	493	513	73
PI/TiO <sub>2</sub> NC4%	515	530	76
PI/TiO <sub>2</sub> NC8%	556	564	78
PI/TiO <sub>2</sub> NC12%	563	576	80

<sup>a</sup> Temperature at which 5 and 10% weight loss was recorded by TGA at heating rate of 20 °C min<sup>-1</sup> in a N<sub>2</sub> atmosphere.

<sup>b</sup> Weight percent of the material left undecomposed after TGA at maximum temperature 800 °C in a N<sub>2</sub> atmosphere.

### Legends for Figures

**Figure 1.** FT-IR spectra of the PAA (a) and PI (b).

**Figure 2.**  $^1\text{H-NMR}$  (400 MHz) spectra of PI in  $\text{DMSO-}d_6$  at R.T.

**Figure 3.** FT-IR spectra of the  $\text{TiO}_2$  NPs (a), PI with 4% (b) and 12% (c) of  $\text{TiO}_2$  NPs and pure PI (d).

**Figure 4.** XRD patterns of  $\text{TiO}_2$  NPs (a), the silane terminated PI (b) and PI with 4% (c), 8% (d) and 12% (e) of  $\text{TiO}_2$  NPs.

**Figure 5.** FE-SEM images of silane terminated PI with 4% (a, b), 8% (c, d) and 12% (e, f) of  $\text{TiO}_2$  NPs.

**Figure 6.** TEM images of silane terminated PI with 4% (a, b) and 12% (c, d) of  $\text{TiO}_2$  NPs.

**Figure 7.** Tensile stress-strain curves of silane terminated PI with different amount of  $\text{TiO}_2$  NPs.

**Figure 8.** TGA thermograms of silane terminated PI with different amount of  $\text{TiO}_2$  NP.

**Figure 9.** UV-visible absorption spectra of silane terminated PI with different amount of  $\text{TiO}_2$  NPs.

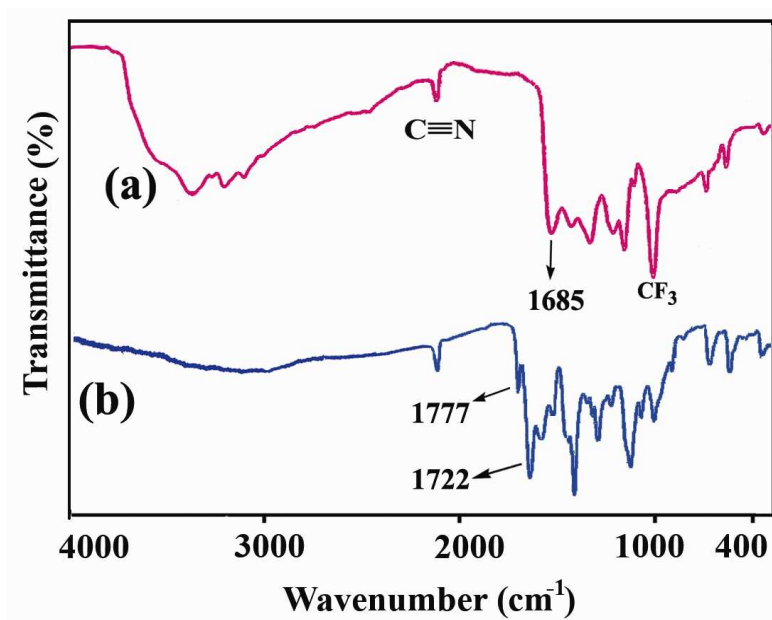


Fig. 1

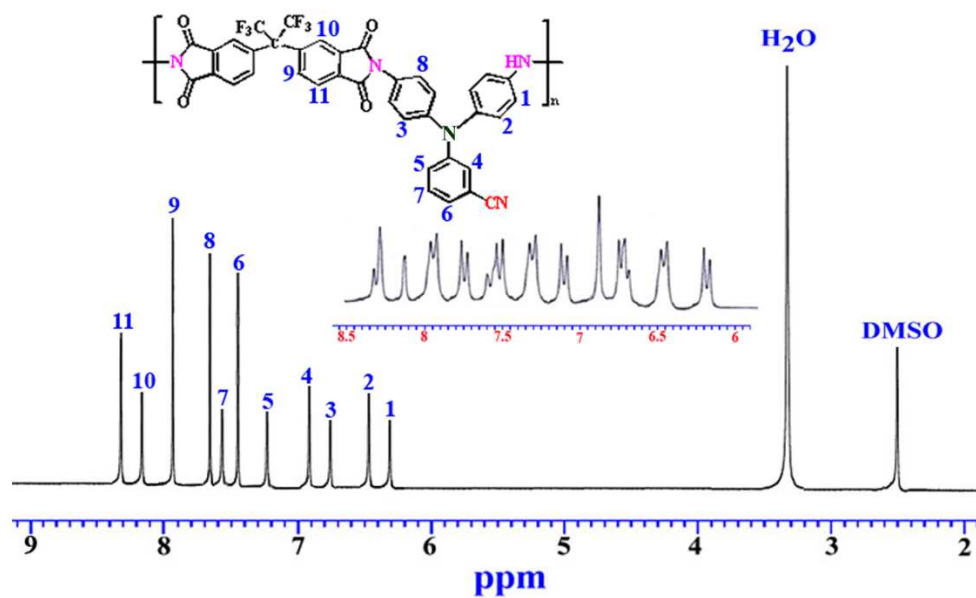


Fig. 2

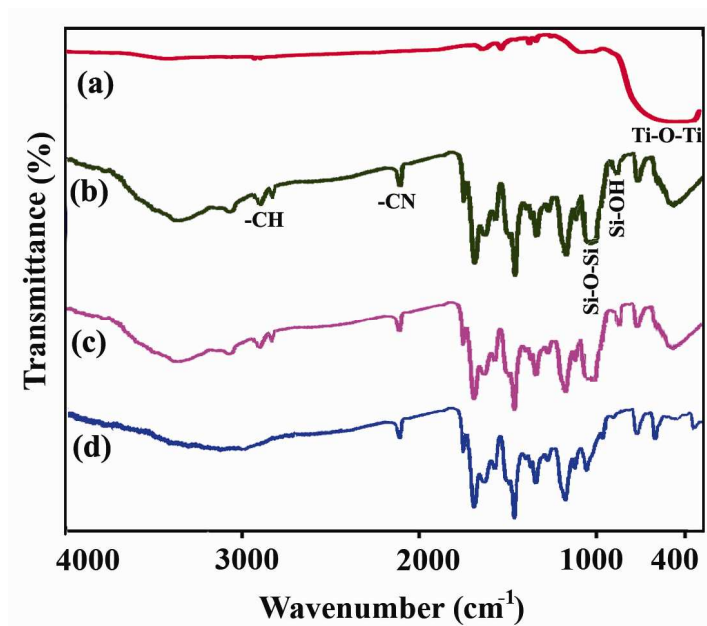


Fig. 3

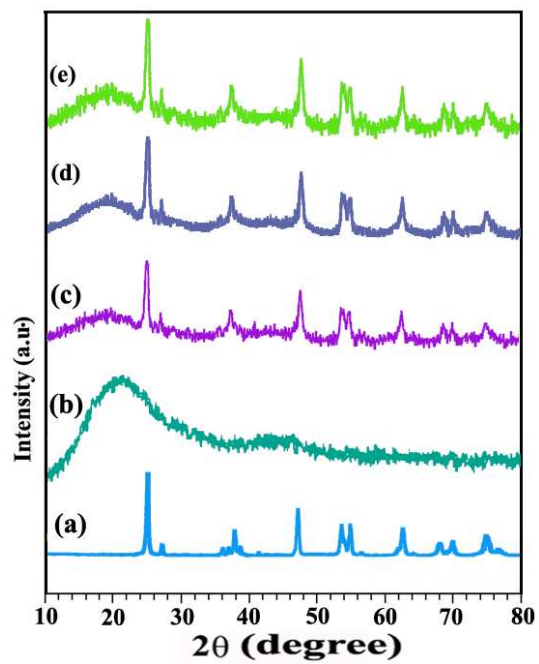


Fig. 4

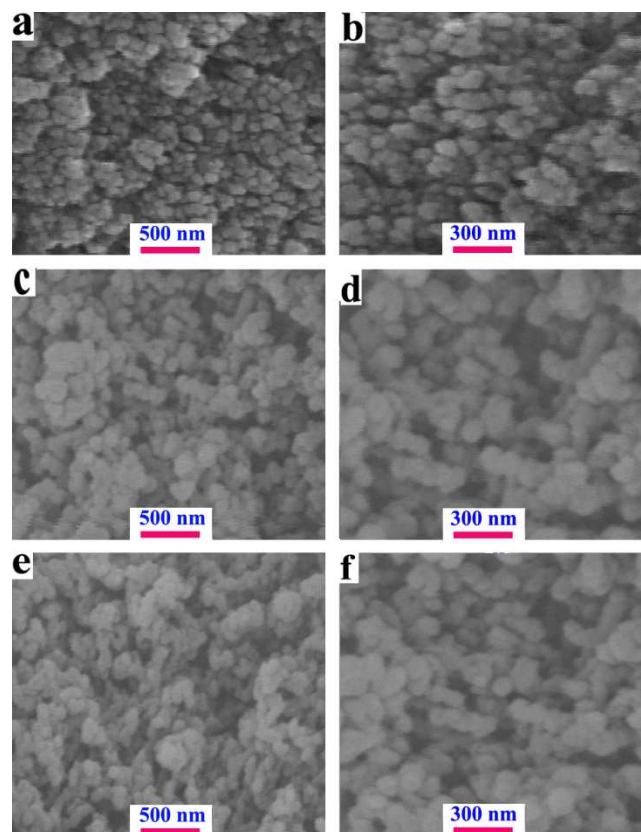


Fig. 5

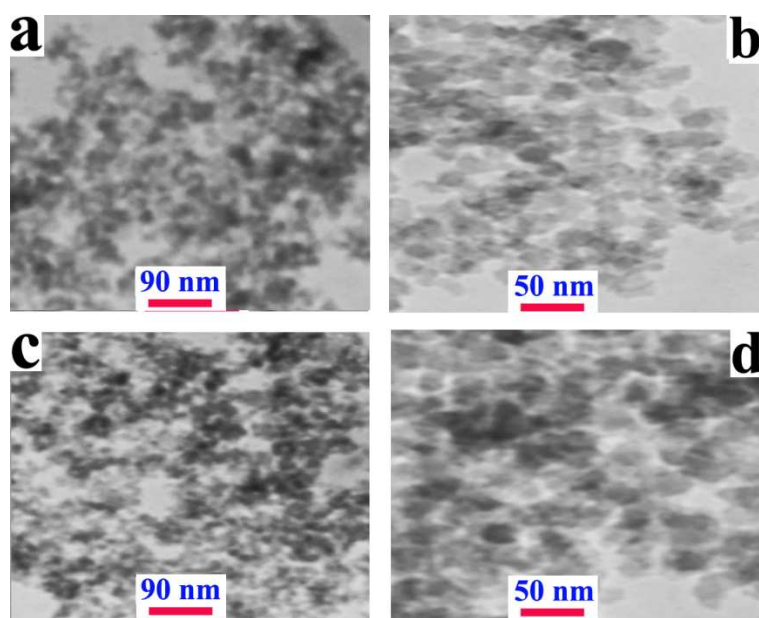


Fig. 6

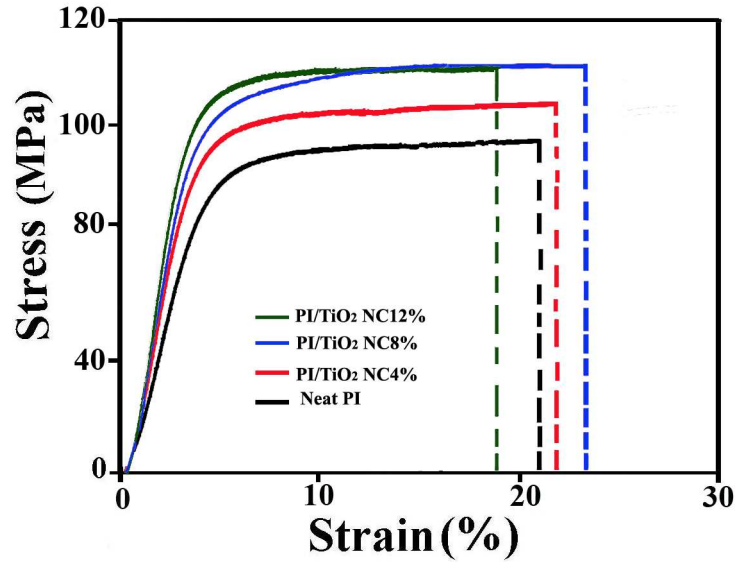


Fig. 7

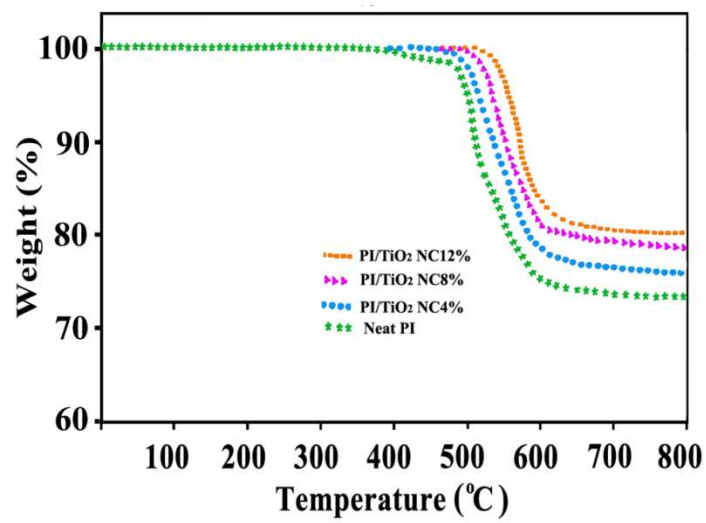


Fig. 8

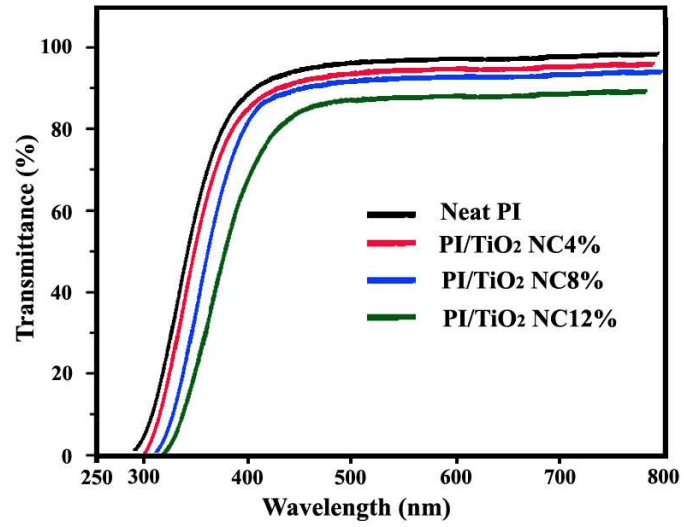


Fig. 9